

CHAPTER 6

Development of SOFC Interconnect Stainless Steels

Sébastien Chevalier^{1,a*}, Lionel Combemale^{1,b}, Ioana Popa^{1,c},
Somrerak Chandra-ambhorn^{2,d}, Walairat Chandra-ambhorn^{3,e},
Piyorose Promdirek^{2,f} and Patthranit Wongpromrat^{3,g}

¹Laboratory ICB UMR 6303 CNRS, Université de Bourgogne Franche-Comté, Dijon, France

²High Temperature Corrosion Research Centre, Department of Materials and Production Technology Engineering, Faculty of Engineering, King Mongkut's University of Technology North Bangkok, 1518, Pracharat 1 Road, Bangsue, Bangkok, 10800, Thailand

³Department of Chemical Engineering, Faculty of Engineering, King Mongkut's Institute of Technology Ladkrabang, Chalongsak 1 Road, Lat Krabang, Bangkok, 10520, Thailand

^asebastien.chevalier@u-bourgogne.fr, ^blionel.combemale@u-bourgogne.fr,
^cioana.popa@u-bourgogne.fr, ^dsomrerak.c@eng.kmutnb.ac.th, ^ewalairat.ch@kmitl.ac.th,
^fpiyorose.p@eng.kmutnb.ac.th, ^gpatthranit.wo@kmitl.ac.th

Keywords: solid oxide fuel cells, interconnect, stainless steel

Abstract. The chapter introduces components and working principle of solid oxide fuel cells (SOFCs). It is followed by the explanation on the choices of materials focussing on ferritic stainless steels. The review is further made on the required properties of these steels, i.e. low oxidation rate, low chromium species volatilisation rate, high electrical conductivity and good scale adhesion. For the oxidation aspect, the behaviour of stainless steel interconnect in cathode, anode (hydrogen and biogas), and dual atmospheres are described. Surface modification by pre-oxidation and coatings to improve the oxide electrical conductivity and to reduce chromium species volatilisation is finally reviewed.

6.1 Introduction

As described by Kofstad and Bredesen, solid oxide fuel cells (SOFCs) are electrochemical reactors for direct conversion of the chemical energy of gaseous fuel and oxygen to electrical energy at high temperatures [1]. Among the various types of fuel cells, SOFCs operate at high temperature, typically between 600 and 1000 °C, and have advantages in terms of high conversion efficiency [2, 3].

Fig. 6.1 schematises the SOFC components and the working principle [4]. A single SOFC cell is generally composed by a porous anode (e.g. YSZ/Ni), a porous cathode (typically a perovskite mixed conductor, e.g. $\text{La}_x\text{Sr}_{1-x}\text{MnO}_3$, $\text{La}_x\text{Sr}_{1-x}\text{Co}_y\text{Fe}_{1-y}\text{O}_3$, etc.) separated by a gas imperviousness ion-conducting electrolyte, such as yttria-stabilised zirconia (YSZ). For the operating principle of SOFCs, oxygen in air on the cathode side received electrons supplied from the anode through the external circuit thus giving oxygen ions (O^{2-}). The oxygen ions transfer from the cathode side through the electrolyte to the anode side. At the anode, hydrogen reacts with oxygen ions giving water and electrons. The flow of electrons through the external circuit gives then electricity.

For the atmospheres on the cathode side, Antoni [4] reported that when air is flowed into this side the partial pressure of oxygen at the inlet is 0.2 bar ($10^{-0.7}$ atm). The oxygen partial pressure can be reduced to about 10^{-4} atm at the gas outlet. It is noted that water vapour can be presented in air and can further affect behaviour of stainless steel interconnect at high temperatures [5, 6]. At equilibrium between liquid and gaseous water vapour, the water vapour content in the atmosphere is in the range of 2.7–3.6% at 20–25 °C calculated using thermodynamic data compiled by Barin [7]. For the anode side, the oxygen partial pressure is considerably low. It can be about 10^{-18} atm at the

gas inlet and increases to be about 10^{-8} atm at the gas outlet. It is noted that in the anode side, the fossil fuel might be used instead of hydrogen since at high temperatures the fossil fuel can be reformed giving hydrogen gas [2, 8]. However, the use of fossil fuel can dramatically change the atmosphere in the anode side compared with the typical one, which mainly contains hydrogen. For example, in the case of methane, gas composition at the inlet is methane but gradually changes to a gas mixture composed of H_2+H_2O and $CO+CO_2$ [1]. At the gas outlet, the partial pressure ratio of CO_2 to CO can be 9:1 and the oxygen partial pressure at 900 °C is 6.7×10^{-15} atm [1]. Furthermore, it was reported that the water vapour content at this location can be as high as up to more than 0.5 atm [1].

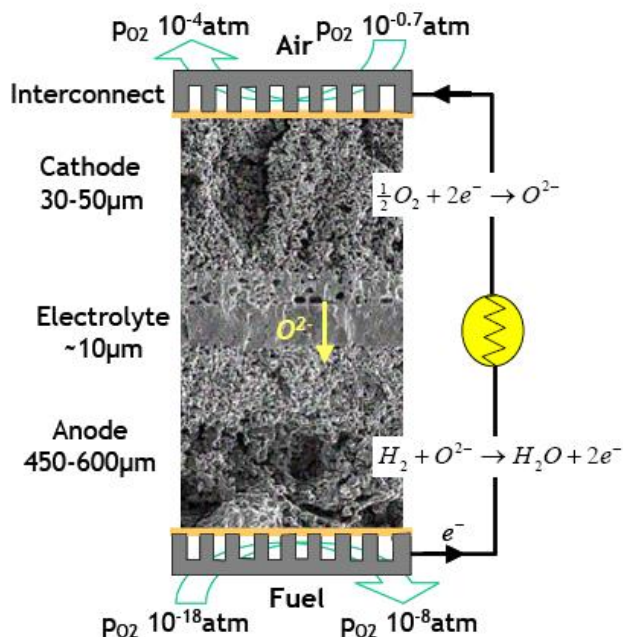


Fig. 6.1. SOFC components and working principle. Reproduced from L. Antoni, Mater. Sci. Forum 461–464 (2004) 1073–1090 [4].

What described above is about a single cell. However, to enhance the voltage output, multiple cells are “stacked” in series. Therefore, an “interconnect” for providing electrical connection between an anode of one individual cell and a cathode of the neighbouring one is required. It also acts as a barrier to avoid any contact between anode atmosphere (hydrogen or fossil fuel) and cathode atmosphere (oxygen or air), while at the same time it helps maintain the structural integrity of the stack.

In order to perform their intended functions, interconnects should have the following characteristics [9–12].

(1) Thermal expansion coefficient (TEC) should match with those of ceramic cell components and seal materials (around $10.5 \times 10^{-6} K^{-1}$), so that the thermal stresses developed during starting up and shutting down could be minimised.

(2) Oxidation and corrosion resistances should be good enough during simultaneous exposure to both cathode and anode atmospheres for 40000 h.

(3) Volatility of constituents that can degrade cell performance should be minimal.

(4) Electrical conductivity, in particular through the oxide scale thermally grown on the metallic interconnect surface, should be high. The acceptable area-specific resistance (ASR) level is considered to be below $100 m\Omega cm^2$ [13].

(5) Scale adhesion should be good so that the separation of scale from the steel substrate, which could lead to electrical resistance, does not occur.

(6) Chemical compatibility with other cell components in contact with interconnects such as seals and electrodes should be good.

In addition, the materials must be cost effective in terms of raw materials and manufacturability. Therefore, the development of suitable interconnect materials is one of challenges in improving the performance and cost-effectiveness of SOFCs.

6.2 Selection of Materials for the Use as an Interconnect

When operating at 900–1000 °C, the leading candidate material for the interconnect was doped lanthanum chromite, $\text{La}_x\text{Sr}_{1-x}\text{CrO}_3$ [4, 14]. However, these materials are quite expensive; moreover, it is difficult to obtain high density at reasonable sintering temperatures and the tendency of the chromite interconnect to be partially reduced at the fuel gas/interconnect interface, causing the component to warp and the peripheral seal to break [2, 15]. The recent trend in developing lower temperature device (650–800 °C), with micrometer thin electrolytes [16], new electrolytes with improved conductivity [17] and/or improvement of the cathode/electrolyte interface reaction (i.e. triple phases boundaries (TPB) to internal diffusion (ID) mechanism) makes it feasible for lanthanum chromites to be supplanted by metals or alloys as the interconnect materials. Indeed, they offer a number of advantages over ceramic materials. They are easier, and therefore cheaper to fabricate, they are less brittle and, in general, they have higher electrical and thermal conductivities compared to the ceramic interconnects [9, 10, 12, 18, 19].

To be reliable, the alloy must develop a thermally grown oxide scale on its surface, which generally has high electrical resistivity. It was reported that electrical conductivity of chromia is about $10^{-1} \text{ S cm}^{-1}$ at 750–800 °C while that of alumina is about $10^{-10} \text{ S cm}^{-1}$ at 700 °C [20]. The relatively high electrical conductivity of chromia can be considered as a “compromise” and lead to the choice of chromia-forming alloys. Among the different groups of chromia-forming alloys (nickel-based, chromium-based and iron-based alloys), the bcc base alloys (chromium-based alloys and ferritic stainless steels) have been the most widely investigated category of alloys for interconnect applications because they have a thermal expansion coefficient ($12 \times 10^{-6} \text{ K}^{-1}$), which matches well with that of ceramic cells ($11 \times 10^{-6} \text{ K}^{-1}$) [18, 19, 21].

Chromium-based alloys, like Plansee Ducralloy, $\text{Cr}_5\text{Fe}_1\text{Y}_2\text{O}_3$, were the early favourites as a replacement for doped lanthanum chromites because they demonstrate excellent oxidation resistance, good electrical properties and high temperature mechanical strength at high temperatures (>900 °C) SOFCs [22, 23]. However, these alloys are very expensive, particularly in comparison with Fe–Cr alloys. In contrast, Fe–Cr ferritic stainless steels (FSS), designated as 400 series in the AISI system, not only demonstrate good oxidation resistance and the ability to match the thermal expansion coefficients of cell components, but also are among the most cost effective alloys [18, 21]. Ferritic stainless steels (e.g. AISI 430, AISI 444, Crofer 22 APU, ZMG 232) were proposed and tested as interconnect materials in stacks in the late 1990s [24].

Traditionally, oxidation resistant alloys have been designed with an emphasis on surface and structural stability, but not electrical conductivity of the scale, which is equally important for SOFC interconnect applications. Thus, alloying practices used in the past to enhance surface and structural stability may not be compatible with high electrical conductivity. For example, silicon that is often a residual element in alloy substrate, may help improve alloy oxidation resistance through formation of silica subscale along the metal/scale interface. This subscale is electrically insulating and therefore increases electrical resistance. It can also cause scale spallation due to its low thermal expansion coefficient, as indicated by studies on ferritic stainless steels such as AISI 446 [25]. Such chromia-forming stainless steels form, at high temperatures, a Cr_2O_3 -based thermally grown oxide (TGO). Unfortunately, the formation of volatile gaseous Cr (VI) species such as CrO_3 or $\text{CrO}_2(\text{OH})_2$ can cause serious degradation of the fuel cell performances by poisoning the cathode and can cause the loss of the protectiveness of chromia [5, 6, 26, 27] especially in presence of water vapour. The formation of a protective, single-phase chromia layer requires chromium content of approximately 17–20%, depending on temperature, on surface treatment and on minor alloying additions [18, 21]. With respect to oxidation behaviour, the most important minor alloying additions in commercial

ferritic steels are manganese, titanium, silicon and aluminium; their concentration commonly being a few tenths of a percent. Manganese was added to obtain external spinel formation, which is expected to decrease the formation of volatile chromium-species and to enhance the electrical conductivity of the scale [28–31]. Titanium was also added to obtain fine internal oxide precipitates of titania leading to strengthening of the near-surface region, thus reducing the tendency of surface wrinkling caused by relaxation of oxidation-related stresses during thermal cycling [24]. The amount of aluminium and silicon must be kept low to prevent the formation of their insulating oxides, alumina and silica. Furthermore, SiO_2 can also cause scale spallation due to its low thermal expansion coefficient, as indicated by studies on ferritic stainless steels [32, 33]. Elements such as tungsten or molybdenum can also be added to match better thermal expansion coefficient of the alloys to those of other fuel cell components. Among newly developed alloys, the one that has received the most attention is Crofer 22 APU, a ferritic stainless steel developed by Quadakkers et al. at Jülich and commercialised by thyssenkrupp of Germany. Crofer 22 APU, which contains ~0.5% manganese, forms a scale composed of a $(\text{Mn,Cr})_3\text{O}_4$ spinel top layer and a chromia sublayer. Besides the “clean” form of ferritic stainless steels that require extra process such as vacuum melting, recent practice has focussed on fabrication of ferritic stainless steels by alloying approach to avoid the negative effects of silica sublayer formation. A small amount of niobium is added to the ferritic substrate and this element ties up residual silicon, mitigating the risk of formation of the insulate silica layer at the metal/scale interface. The niobium-containing ferritic stainless steel, as AISI 441, demonstrates an electrical performance comparable to Crofer 22 APU [34, 35].

Table 6.1 exemplifies commercial ferritic stainless steel grades for interconnect application [5, 36–39]. It can be seen from the table that the basic grade is AISI 430, which mainly consists of iron with 16.5 wt.% chromium. The higher grades in this series are AISI 441 and 444, which contains higher chromium content of about 18 wt.%. In general, the chromium contents are in the ranges of 17.5–18.5 wt.% and 17–20 wt.% for AISI 441 and 444 respectively [40]. The AISI 444 is also stabilised by titanium but additionally alloyed with molybdenum by about 2 wt.%. It was reported that the molybdenum addition could help increase the pitting corrosion resistance [41], the stress corrosion resistance [42], the cyclic oxidation and high temperature strength of the steel [43–45]. However, as will be shown in Section 6.6, the molybdenum addition could form Fe–Mo intermetallic compound, which deteriorates the scale adhesion at high temperatures [36].

Table 6.1 Chemical compositions (wt.%) of ferritic stainless steels for SOFC interconnect application [5, 36–39].

Grade	Cr	Other elements	Ref.
430	16.5	0.4Mn–0.35Si	[5]
441	17.8	0.24Mn–0.6Si–0.006Al–0.13Ti–0.55Nb	[36]
444	17.6	0.42Mn–0.42Si–2.04Mo–0.16Ti–0.28Nb	[36]
Crofer 22 A	22	0.5Mn–0.1Si–0.1Al–0.1Ti–0.1La	[37]
Crofer 22 APU	22	0.5Mn–0.02Si–0.02Al–0.1Ti–0.1La	[37]
Crofer 22 H	22	0.5Mn–0.25Si–0.02Al–0.1Ti–0.1La–2W–0.5Nb	[37]
ZMG 232	22	0.5Mn–0.4Si–0.21Al–0.22Zr–0.04La–0.26Ni	[37]
ZMG 232L	21.8	0.46Mn–0.08Si–0.05Al–0.19Zr–0.05La–0.34Ni	[38]
ZMG 232 G10	23.6	0.27Mn–0.05Si–0.08Al–0.32Zr–0.06La–0.51Ni–1.99W–0.96Cu–0.02N	[39]
Sanergy HT	22.3	0.24Mn–0.02Si–0.03Al–0.77Mo–0.03Ti–0.6Nb–0.1Zr	[37]
ITM	25.7	0.04Mn–0.03Si–0.04Al–1.9Mo–0.21Ti–0.24Y	[37]
E-bright	26	0.05Mn–0.2Si–1Mo–0.1Nb–0.15Ni	[37]

The next ferritic grades with higher chromium content are the grades with about 22 wt.% chromium. The major grades specially developed for this application are Crofer and ZMG. As previously mentioned, the Crofer grade has been developed by Jülich Research Centre and commercialised by thyssenkrupp. Niewolak et al. reported that Crofer 22 A stainless steel mainly consists of iron with 22 wt.% of chromium, also with 0.1 wt.% of lanthanum as a reactive element and 0.1 wt.% of titanium. Silicon and aluminium contents in this grade are equally 0.1 wt.%. The Crofer 22 APU still contains the same contents of chromium, lanthanum and titanium. However, the silicon and aluminium contents of this grade are reduced to be 0.02 wt.%. Furthermore, in order to increase the creep strength of this stainless steel, tungsten with the content of 2 wt.% is added to Crofer 22 APU with slight modification of the chemical compositions of the other elements, giving rise to the Crofer 22 H grade [37]. The ZMG grade has been developed by Hitachi Metals. This grade also contains chromium content of about 22 wt.% but it is added by the reactive elements i.e. zirconium and lanthanum. It is noted that the silicon and aluminium contents of this steel are relatively high i.e. 0.4 and 0.21 wt.%, respectively [37]. The contents of these two elements were reduced to be 0.08 and 0.05 wt.% for the improved ZMG 232 L [38]. Recently, new ZMG 232 G10 has been developed still with the reduced silicon and aluminium contents but additionally with about 2 wt.% of tungsten, 1 wt.% of copper and 0.02 wt.% of nitrogen [39].

The ferritic grades with higher chromium content of 25–26 wt.% are such as ITM and E-bright as shown in Table 6.1. Similar to the steel with lower chromium contents, these grades tend to be produced by lowering the silicon and aluminium contents and alloying molybdenum, titanium, niobium or the reactive elements such as yttrium. However, the steels with chromium content higher than 25 wt.% are prone to precipitate the sigma phase even at the high temperature of 800 °C if some other elements, e.g. molybdenum and silicon, are added to the steel [46]. Singheiser et al. [46] then recommended that the chemical composition of the high-chromium steel must be carefully adjusted to the actual environment to avoid the sigma phase formation, which could cause the embrittlement of the steel.

6.3 Oxidation Behaviour

6.3.1 Oxidation on the Cathode Side

During high temperature exposure in air, chromium contained in the alloy substrate is preferentially oxidised, forming an oxide scale on the alloy surface to protect it from further environment attack. Some studies revealed that, in most cases, outward chromium transport is the dominant growth process in the chromia scale, whereas the contribution of oxygen transport is substantially smaller [47, 48]. However, stainless steel does not contain only chromium but also manganese. The latter element can play a role on oxidation kinetics. Park et al. [49] have recently studied the air oxidation mechanism of Crofer 22 APU and found that the oxidation mechanism composes of two steps. In the first step, Cr–Mn spinel and chromia are grown with the faster rate for the spinel formation because of the rapid outward diffusion of manganese [49]. Later, when oxygen penetrates through the spinel layer and reaches the chromia, the growth rate of chromia is changed abruptly and becomes faster than the growth rate of spinel [49]. This mechanism finally leads to the formation of chromia as a major scale with the relatively thin Cr–Mn spinel formed on the top of chromia.

Furthermore, the outward chromium diffusion results in the formation of voids and cavities at the metal/scale interface leading to poor scale adherence. Thus, after exposure over thousand hours, the chromia layer can exhibit localised spallation and thus creates an important electrical power loss at the electrode/interconnect interface [21, 50, 51]. It is well known that the addition of small amounts of reactive elements (lanthanum, zirconium, yttrium, neodymium, etc.), to Cr₂O₃-forming alloys greatly enhances their resistance to high temperature oxidation [47, 48, 52]. This effect, known as reactive element effect, is reviewed in Chapter 4. However, it may be briefly described here that their main role consists of changing the diffusion mechanism during the chromia scale formation

from outward diffusion of the chromium ions to inward diffusion of the oxygen ions. The change of the diffusion mechanism allows for the decrease of the corrosion rate and can significantly increase the oxide scale adherence. The reactive element effect can be produced by a wide variety of reactive element addition methods, such as microalloying [21], dispersion of oxides [25] and surface coatings with a thin layer of the reactive element oxide [23, 53]. The enhancement of the electrical properties by addition of reactive element was also observed [23, 53].

6.3.2 Oxidation on the Anode Side

6.3.2.1 Oxidation in H₂-H₂O

In comparison with the oxidising, cathode side environment, the reducing, anode side environment is more complex, particularly when a hydrocarbon fuel is used. However, the understanding of the oxidation behaviour in anode environment (H₂-H₂O) is very important and it is still lacking. The literature data dealing with the effect of water vapour on chromia-forming alloys show that water vapour plays a huge role on the corrosion phenomenon. The water vapour seems to be either beneficial or detrimental. Concerning the corrosion rate, some papers are contradictory [54]. Brylewski et al. [55] reported similar values of k_p for oxidation of AISI 430 in air and in 94% H₂/6% H₂O but the electrical resistance was higher in the anode gas than in the cathode gas. On one hand, Quadackers et al. [56] reported that the chromia scales formed on ferritic stainless steels in simulated anode gas at 800 °C were thinner than those formed in air. On the other hand, although the oxygen partial pressure was lower on the anode side, Quadackers et al. [56] also found that the oxidation rate of chromium-based ODS alloy at 950–1050 °C in a H₂/H₂O mixture (equilibrium oxygen partial pressure approximately 10–15 bar) was higher than in the environments with high oxygen partial pressure (air, Ar/O₂). England and Virkar [57] oxidised nickel-based alloy (Haynes 230) in H₂-H₂O and in air between 700 and 1100 °C. The growth rate of the chromia scale at 800 °C in H₂-H₂O was higher than that observed in air; moreover, the electrical resistance of the scale was higher in H₂-H₂O than in air. Liu [58] also found that, in a reducing atmosphere of Ar-5% H₂-3% H₂O, the electrical property of the oxide scale was worse. Finally, Fontana et al. [53] found that in a reducing atmosphere H₂-10% H₂O, the corrosion rates of Crofer 22 APU and Fe-30Cr were higher than those in air atmosphere. Due to the technical difficulty to measure electrical resistance in H₂-H₂O, the electrical property of the thermally grown oxide in H₂-H₂O is not well understood. Guillou et al. [59] evidenced in solid oxide electrolyser (SOE) conditions and by using marker experiments with D₂O that it was the hydrogen coming from water vapour that was the main cause of the drastic decrease of the electrical conductivity of chromia scale. One beneficial effect of water is that it can improve the adherence of the scale [36, 60], especially during thermal cycling, by reducing the amount of porosity at the alloy/scale interface. The severe buckling of the scale formed on chromia-forming alloy without reactive element observed by many authors during air oxidation does not occur during oxidation in H₂-H₂O. For example, oxide scale formed on chromia-forming alloy in H₂-H₂O showed good adhesion during cyclic oxidation at 950 °C, whereas scale formed in air in the same condition showed spallation [24]. Conversely, on the outer part of the scale, water vapour was shown to promote the formation of less protective microporous scale [24, 61].

6.3.2.2 Oxidation in Biogas

As mentioned in Section 6.1, one of the advantages of SOFC is that the fossil fuel might be used since it can be reformed at the SOFC working temperature thus providing hydrogen gas for the anode side. One of the promising types of renewable fuel is biogas. The biogas issued from fermentation typically contains about 50–70% methane, 30–50% CO₂ with H₂S as impurity [62, 63]. To understand the high temperature corrosion mechanism of stainless steel under biogas, the corrosion mechanism of stainless steel under CO₂ was first explored and then followed by CO₂ mixed with methane which is in fact the biogas.

For the AISI 441 stainless steel oxidation in dry CO₂, Promdirek et al. [64] found that at 700–850 °C the oxidation kinetics was linear, while at higher temperatures i.e. 925–1000 °C the oxidation was firstly linear followed by parabolic at longer times [64]. At the SOFC working temperature of 800 °C, they found that the relationship between the linear rate constant (k_1) and CO₂ partial pressure (p_{CO_2}) was in the following form:

$$k_1 = \frac{Ap_{\text{CO}_2}}{1 + Bp_{\text{CO}_2}} \quad (6.1)$$

where A and B are constant. Furthermore, they found from the photoelectrochemical experiment that the oxide formed in this atmosphere was n-type [64]. Based on these results, the oxidation mechanism in CO₂ was proposed as follows.

First, CO₂ adsorbs on the metal surface i.e.



where s is the available site on the surface and CO₂–s is the adsorbed CO₂ [64].

Second, the adsorbed CO₂ dissociates giving the adsorbed oxygen and CO according to the following reaction [64]:



If it is considered that $V_{\text{O}}^{\bullet\bullet}$ is a dominant defect in this condition, this defect could be formed at the metal/scale interface by the following reaction:



where $<\text{Cr}>$ is the chromium in stainless steel and Cr_{Cr} is chromium on the chromium site in chromia. The formed $V_{\text{O}}^{\bullet\bullet}$ diffuses to the external interface. Such defect is filled by the adsorbed oxygen in Reaction 6.3 giving



In the case that Reaction 6.3 is a rate determining step, the reaction rate (r) is as follows [64]:

$$r = k_{6.3}\theta \quad (6.6)$$

where $k_{6.3}$ is the rate constant of Reaction. 6.3 and θ is the coverage ratio of CO₂ on the surface. If equilibrium of Reaction 6.2 is assumed, we can write the equilibrium constant as

$$K_{6.2} = \frac{\theta}{p_{\text{CO}_2}(1-\theta)} \quad (6.7)$$

From Eqs. 6.6 and 6.7, we can obtain that

$$r = \frac{k_{6.3} K_{6.2} p_{\text{CO}_2}}{1 + K_{6.2} p_{\text{CO}_2}} \quad (6.8)$$

This reaction rate is in the same form of the relationship between the linear rate constant and the CO₂ partial pressure, as experimentally found in Eq. 6.1. This congruence supports the feasibility of the proposed mechanism [64].

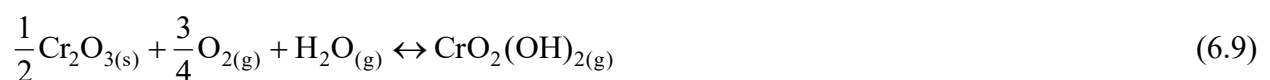
Further, when methane is added to CO₂ by 30–70% at 700–900 °C, Promdirek et al. [63] found that the corrosion kinetics was linear and the linear rate constant increased with the increased ratio of methane in the biogas. They proposed that the high temperature corrosion of AISI 441 stainless steel in biogas was due to two parallel mechanisms: the oxidation by CO₂ and the carburisation by methane. They further reported that the carbon deposition and carbide formation were very rapid in pure methane. This phenomenon should contribute to the faster corrosion rate in biogas with the higher proportion of methane as observed from the experiment [63]. From the experiment, they further found that the scale was compact at 700 and 800 °C and could act as a barrier for carbon penetration, while at the higher temperature of 900 °C the scale was porous and carbide was formed near the metal/scale interface which could lead to the embrittlement of the steel. The SOFC working temperature of 800 °C seems then to be the maximum temperature for the use of AISI 441 stainless steel in this biogas atmosphere [63].

6.3.3 Oxidation in Dual Exposure Conditions

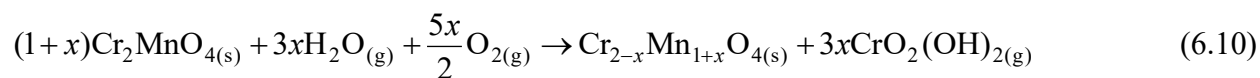
When simultaneously exposed to air at the cathode side and to H₂-H₂O at the anode side during SOFC service, interconnects experience a hydrogen partial pressure or chemical potential gradient from the fuel side to the air side. The oxidation behaviour in dual environment is very important and it is still lacking. Yang et al. [65, 66] observed that the oxidation behaviour of an alloy exposed to wet hydrogen on one side and air on the other side was different from that exposed to air on both side. The scales formed in air on AISI 430 exposed to a dual atmosphere contained iron-rich spinel or Fe₂O₃ nodules. In comparison, there was no haematite phase formation on the air/air sample, on the hydrogen side of the air/hydrogen sample, or on the hydrogen/hydrogen sample. This anomalous oxide (haematite instead of chromia) in air side was described in literature in dual atmosphere [67–74]. The potential detrimental effect of the dual exposure appeared to be dependent on the alloy composition, in particular chromium percentage in the Fe–Cr substrate. For Crofer 22 APU with 22 wt.% chromium, no haematite phase formation was observed under the same test conditions as for AISI 430. The mobility of iron in chromia is higher than that of chromium [75], but the oxidation behaviour in a dual atmosphere suggests that hydrogen may further increase the mobility of iron. Measurements of the permeation of hydrogen through ferritic stainless steels [76] indicate that hydrogen can diffuse through the sample. However, the permeability of hydrogen through chromia is low, so once a protective chromia scale forms, the amount of hydrogen penetrating through oxidised sample is low. This anomalous behaviour in dual condition was found to be emphasised by electrical current in SOE conditions [77]. The mechanism of this phenomenon is not very clear and further work is required to gain further insight into the oxidation behaviour under dual environment and its effects on long term metallic interconnect stability.

6.4 Chromium Species Volatilisation

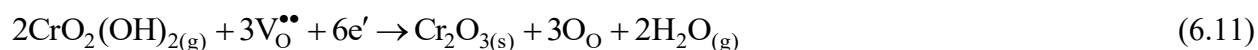
On the cathode side where the oxidising atmosphere is humidified, the chromia formed on stainless steel does not only oxidise but could also volatilise. At temperatures lower than 1500 °C, the dominant reaction of the volatilisation of chromia by oxygen and water vapor was reported to be the following one [5, 6, 78]:



In the case of stainless steel which contains not only chromium but also manganese, the addition of manganese could lead to the formation of Cr–Mn spinel on the top of chromia layer. In this case, the chromium volatilisation from the Cr–Mn spinel could be as follows [79, 80]:



It was reported that the $\text{CrO}_2(\text{OH})_2$ volatile species could diffuse through the porous cathode to the interface between cathode and electrolyte and reduced there giving chromium oxide, possibly by the following reaction [81]:



The precipitation of this oxide blocks the active sites for oxygen reduction at the cathode/electrolyte interface, thus degrading the cell performance. In the case that the cathode is LSM, the oxide $(\text{Cr},\text{Mn})_3\text{O}_4$ can also be formed at the interface between the cathode and electrolyte [81, 82]. This problem can be reduced by forming the oxide scale that exhibits low chromium volatilisation rate, which can be done by adding some alloying elements, by pre-oxidation before using the alloy in service, or by appropriate coating. The two first methods will be described in the following while the last method will be described in Section 6.7.

As for the effect of the alloying element, the important element for suppressing the chromium volatilisation is manganese. Galerie calculated the partial pressure of the chromium volatile species i.e. $\text{CrO}_2(\text{OH})_2$ from chromia (Cr_2O_3) and Cr–Mn spinel (MnCr_2O_4) in N_2 -20% O_2 -15% H_2O at 900–1500 °C [40]. Thermodynamic data for Cr_2O_3 , MnCr_2O_4 came from Opila [78] and Jung [83], respectively. It was found that the partial pressure of $\text{CrO}_2(\text{OH})_2$ from Cr_2O_3 is in the range of 1.6×10^{-7} to 3.7×10^{-6} bar, while the partial pressure of $\text{CrO}_2(\text{OH})_2$ from MnCr_2O_4 is lower in the range of 5.2×10^{-9} to 3.5×10^{-7} bar. It indicates the possibility that the chromium volatilisation rate from the scale containing Cr–Mn spinel is lower than that containing only chromia.

For the chromium volatilisation from alloys, Niewolak et al. [37] compiled the results from literature [84, 85] and empirically found that the increase of manganese in various alloys up to about 0.5 wt.% could lead to the reduced chromium species volatilisation rate. It is widely accepted that the formation of Cr–Mn spinel could suppress the chromium species volatilisation from stainless steel [5, 37]. However, the protectiveness from chromium species volatilisation due to Cr–Mn spinel is not only from the formation of continuous layer but also the chromium-to-manganese ratio in this oxide. In this matter, Falk-Windish et al. [80] reported that the ratio of chromium to manganese in Cr–Mn spinel i.e. $(\text{Cr},\text{Mn})_3\text{O}_4$ can vary from 2:1 to below 1:2. In the early period of oxidation, this ratio is relatively high, but it gradually decreases due to the rapid outward manganese diffusion and approaches a constant value. The decrease in this ratio implies the lower chromium activity and thus the lower chromium species volatilisation rate.

For the pre-oxidation technique, stainless steel might be oxidised in a reducing atmosphere to give the n-type chromia [6, 64]. In the case that the dominant defect at the external part of the chromia is a p-type metal vacancy, the hydroxyl ion cannot jump into the metal vacancy site [6]. On the contrary, if the dominant defect in chromia is an n-type oxygen-vacancy, the hydroxyl ion could be easily incorporated into the oxide, as shown in Fig. 6.2 [6]; in such a case that the chromium species volatilisation could be suppressed. Such possibility to reduce chromium species volatilisation is congruent with the experiment conducted by Wongpromrat et al. [6]. They pre-oxidised AISI 441 stainless steel in 50% CO -50% CO_2 atmosphere at 850 °C to let the formation of n-type oxide, and found that the pre-oxidation could help reduce the chromium specie volatilisation rate of the steel in O_2 -5% H_2O at 800 °C [6]. For example, at the linear gas velocity of 4 cm s^{-1} ,

the chromium species volatilisation rate of the bare AISI 441 is about $2 \mu\text{g m}^{-2} \text{s}^{-1}$. It reduces to about $0.25 \mu\text{g m}^{-2} \text{s}^{-1}$ when the mentioned pre-oxidation was conducted [6].

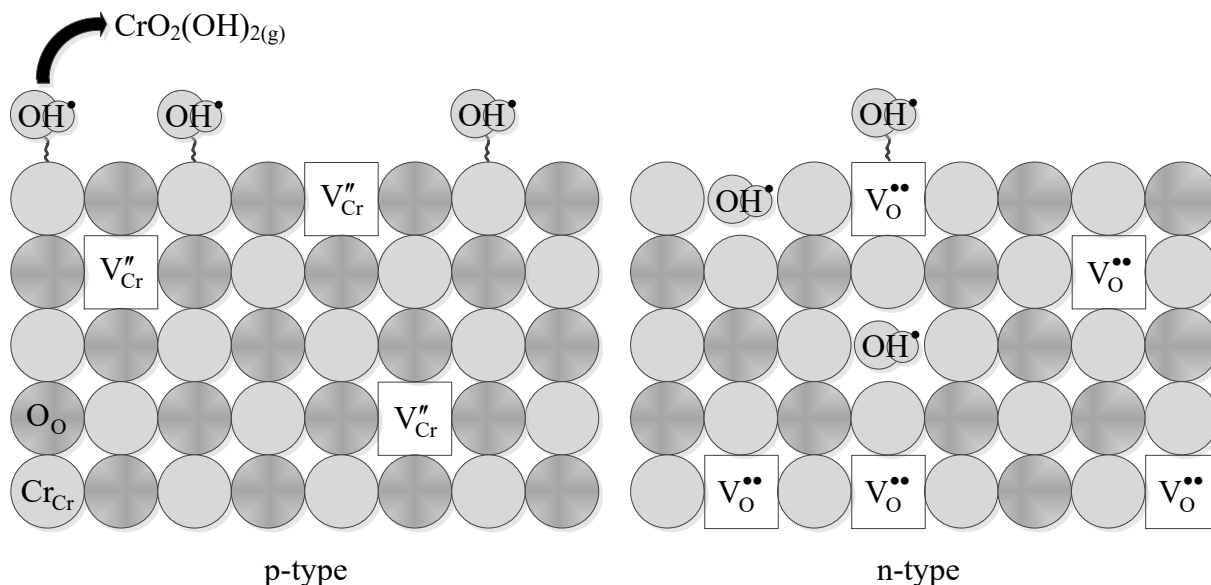


Fig. 6.2. Effects of metal vacancy (left) and oxygen vacancy (right) in the oxide on the chromium species volatilisation. Redrawn from Wongpromrat et al., Corros. Sci. 106 (2016) 172–178 [6].

6.5 Area Specific Resistance

Electrical resistivity of the oxide (ρ_o) follows the basic relation $\rho_o = RA/l_o$ where R is the electrical resistance of the oxide, A is the surface area of the oxide that electric current passes through, and l_o is the oxide thickness. From this relation, the area specific resistance (ASR) is defined as follows [86, 87]:

$$ASR = \rho_o l_o = RA \text{ (}\Omega \text{ cm}^2\text{)} \quad (6.12)$$

This parameter is widely used to assess the electrical property of thermally grown oxide on metal because it simultaneously takes into account the proper electrical property (i.e. the resistivity of the oxide, ρ_o) and the oxidation kinetic parameter (i.e. the oxide thickness, l_o) that is increased during oxidation [86, 87]. This parameter can be obtained by measuring R and A from the experiment. In the ASR measurement, if the interfacial electrical resistances between metal and electrodes are negligible, the electrical resistance measured from the experiment is attributed to the resistance of oxide and metal. The resistance of metal is significantly lower than that of the oxide as Huang et al. reported that the resistivity of Fe–26Cr–1Mo at 900 °C was $0.0141 \text{ m}\Omega \text{ cm}^2$ [87]. Thus, the measured electrical resistance can be considered as the electrical resistance of the oxide (R) [87].

Fig. 6.3 shows ASRs of the bare ferritic stainless steels after oxidation at 800 °C in air [88–94]. The first and second bars from the left present, respectively, the results after 100 and 200 h of exposure. The other bars present the results after 300 h of exposure. After the 300 h exposure, it can be seen that stainless steel (Fe–17Cr) with 1 wt.% of aluminium exhibits the highest ASR of about $20000 \text{ m}\Omega \text{ cm}^2$ [91]. The ASR of AISI 441 is about $30 \text{ m}\Omega \text{ cm}^2$ [91, 92], similar to that of ZMG 232 [91]. The model alloys in a family of FeCrMn(La/Ti) leading to the development of Crofer 22 APU have ASRs in the range of $10\text{--}15 \text{ m}\Omega \text{ cm}^2$ [91] lower than the ASR of Crofer 22 APU which is in the range of $35\text{--}50 \text{ m}\Omega \text{ cm}^2$ as reported by Hosseini et al. [93] and Ebrahimifar and Zandrahimi [94]. At shorter oxidation period i.e. 100 h, the ASR of Crofer 22 APU was also reported to be

about $50 \text{ m}\Omega \text{ cm}^2$ [88]. For AISI 430, the ASR was reported to be about $35 \text{ m}\Omega \text{ cm}^2$ after the exposure for 200 and 300 h [89, 90].

Many methods can be done to decrease the ASR of ferritic stainless steels. *The first method* is to dope the elements that could lead to the generation of electron in the conduction band of the oxide. For example, the titanium in titania may be doped into chromia by the jumping of titanium into the site of chromium in chromium oxide giving $\text{Ti}_{\text{Cr}}^\bullet$ and $\text{Cr}_i^{\bullet\bullet}$. The formation of these defects are accompanied by the generation of electron presumably by Reaction 6.13, thus increasing the electrical conductivity of the oxide as experimentally observed in the titanium doping into the oxide thermally grown on AISI 441 [86]. However, it is noted that the titanium doping could not only increase the electrical conductivity of the oxide but also enhanced the steel oxidation rate [86]. The other methods are further looked for to decrease the ASR.

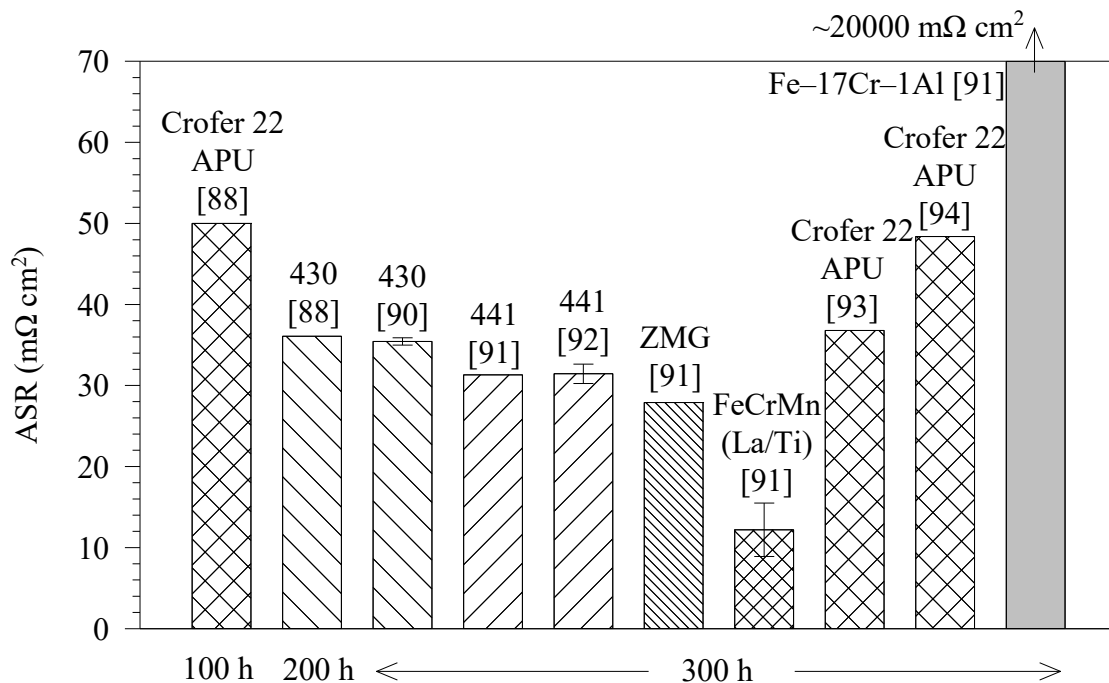


Fig. 6.3. Area specific resistance of ferritic stainless steel interconnects in air at 800 °C [88–94].

The second method to decrease ASR is to add the elements to promote scale adhesion. This is to avoid the separation of the scale from steel substrate which further results in the formation of air gap which has an infinite electrical resistivity. However, this addition must also be optimised with the possible altered oxidation rate. The roles of element on altering the scale adhesion will be described in the next section. *The last method* consists in covering the surface by a conductive coating that also enables to limit chromia formation.

6.6 Scale Adhesion

Scale adhesion can be affected by steel chemistry and gas composition in the atmosphere. For the steel chemistry effect, some elements e.g. lanthanum, molybdenum, titanium and niobium are added to stainless steels as seen in Table 6.1 and could affect the scale adhesion. Many testing methods have been developed to assess the scale adhesion test (as reviewed in Chapter 2). In this section, the adhesion test using the tensile method is described. The studied sample is placed in a micro-tensile

machine which is situated in a SEM chamber. The sample is strained in the SEM chamber at room temperature and the evolution of scale failure is observed during straining. At a given strain after spallation takes place, the spalled area is measured and normalised by the total area of the taken image, giving the spallation ratio. This parameter is used to assess the scale adhesion in the manner that higher spallation ratio indicates worse scale adhesion.

Fig. 6.4 shows the surface of AISI 441, 444 and Crofer 22 APU oxidised in simulated atmospheres at cathode side (synthetic air) and anode side (H_2 -2% H_2O) of SOFCs at 800 °C for 200 h, after straining by the similar strain [36, 86]. The tensile loading was applied in the horizontal direction for the samples shown in this figure. It can be seen that the scale on Crofer 22 APU is best adhered to the steel substrate because the scale is failed only by the transverse crack without spallation on the major part of the oxide. This should be from the effect of reactive element i.e. lanthanum added to the steel. The scale on AISI 444 is badly adhered to the steel substrate as the high spallation ratio is observed in both atmospheres. After spallation in humidified hydrogen, Fe_3Mo_2 intermetallic compound was observed on the metal side at the internal interface between scale and the AISI 444, congruent to the thermodynamic prediction [36]. The formation of this compound is believed to be responsible to the worse scale adhesion.

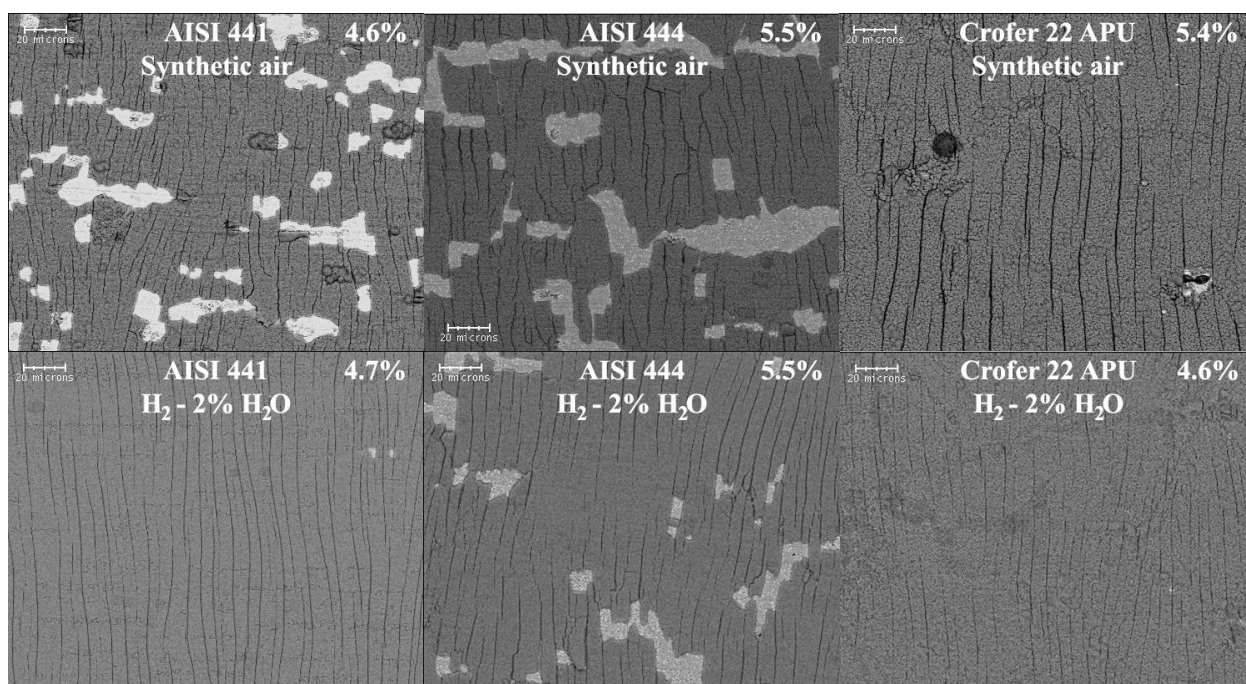


Fig. 6.4. Top view of the scales on AISI 441, AISI 444 and Crofer 22 APU oxidised at 800 °C in synthetic air (first row) and H_2 -2% H_2O (second row) after tensile testing using the similar imposed strain. Reproduced from S. Chandra-ambhorn et al., *J. Power Sources* 171 (2007) 688–695 [36] and S. Chandra-ambhorn, PhD Thesis, INP Grenoble, France, 2006 [86].

As for the effect of gas composition in the atmosphere on scale adhesion, Fig. 6.4 shows the surface of AISI 441 and 444 oxidised in different atmospheres (synthetic air and H_2 -2% H_2O) after straining by the similar strain. It can be seen that water vapour can promote the scale adhesion as for each grade the spallation ratio is less when it is oxidised in humidified atmosphere. It was proposed that water vapour could be dissociated to be hydroxyl ion [36, 95]. This species dissolves in the oxide and rapidly diffuses to the internal steel/scale interface because the ionic radius of the hydroxyl ion is less than that of the oxygen ion [36, 95]. As a result of the hydroxyl ion inward diffusion, scale is formed at the steel/scale interface, thus promoting the adhesion [36, 95].

6.7 Influence of Coatings

As an alternative approach to the bulk modification of alloys, a metallic interconnect can be surface-modified via a protective oxide layer. The protective layer is particularly important on the cathode side due to the oxidising environment and the susceptibility of SOFC cathodes to chromium poisoning. The protection layer is intended first to serve as a barrier to both chromium cation outward and oxygen anion inward diffusion, so that it can decrease the alloy oxidation kinetics and mitigate or even prevent chromium migration and formation of Cr (VI) oxide and oxide-hydroxide. Secondly, the protection layer helps minimise the area specific resistance between electrodes and interconnect by limiting the growth of the chromium-based oxide scale, which has relatively low conductivity. The promising coating materials for these purposes are at least perovskite or spinel coatings.

Perovskite has a formula of ABO_3 . A is a trivalent rare earth cation e.g. lanthanum, strontium and yttrium, while B is a transition metal cation such as chromium, manganese, cobalt, iron, copper and nickel [96]. It was reported that the compositions of iron, copper, nickel could be adjusted to increase the oxide electrical conductivity and TEC compatibility [10, 96]. The examples of perovskite compounds are lanthanum chromite ($LaCrO_3$), lanthanum strontium chromite ($La_{1-x}Sr_xCrO_3$), lanthanum strontium manganite ($La_{1-x}Sr_xMnO_3$), lanthanum strontium cobalite ($La_{1-x}Sr_xMnO_3$) and lanthanum strontium ferrite ($La_{1-x}Sr_xMnO_3$). [96]. It was reported that the addition of strontium to the $LaCrO_3$, $LaCrO_3$ or $La(Co,Fe)O_3$ could significantly increase the electrical conductivity of these oxides [97]. However, even though the doped $LaCrO_3$ with p-type conducting property exhibits high electrical conductivity in the oxidising atmosphere [96, 98], its conductivity could be significantly reduced in a reducing atmosphere [10, 98]. Shaigon et al. [99] also commented that the perovskite coatings could allow the oxygen to transport to some extent and that it was difficult to develop a fully dense layer. Reactive element oxides could be coated to provide the reactive element effect including the reduced oxidation rate of the alloys. Fontana et al. [100] demonstrated that the addition of a nanometric reactive element oxide (La_2O_3 , Y_2O_3) layer applied by Metal Organic Chemical Vapour Deposition (MOCVD) drastically improved both corrosion rate and electrical properties in air of Crofer 22 APU and Haynes 230 alloys even after 20 months exposure at 800 °C in air. During aging in SOFC conditions, La_2O_3 transformed into $LaCrO_3$. This underlying $LaCrO_3$ perovskite layer contributed to better electrical behaviour, but was able to dope the chromia layer grown at the alloy surface, providing then the well known “reactive element effect” [101, 102].

For the spinel coating, this compound has a formula of AB_2O_4 . A and B could be di-, tri- or quadri-valent cations in octahedral or hexahedral sites, while O is an oxygen anion located at face-centre-cubic lattice sites [96]. The types of elements and compositions of A and B can be adjusted to give the spinel with TEC compatible to the chromia and high electrical conductivity. Petric and Ling [103], and Paknahad et al. [104] measured these two properties when A and B were various elements as shown in Figs. 6.5 and 6.6.

Fig. 6.5 presents the TEC of AB_2O_4 spinel at 800 °C where the elements shown in x-axis are B. Different bars at a certain B element x-axis present the TEC of spinels consisting of different A elements. All spinels in the figure have a formula of AB_2O_4 except Cu–Mn spinel which has a formula of $Cu_{1.3}Mn_{1.7}O_4$. It can be seen that most of the spinels which B is Fe tend to have the TEC in the range of about 11×10^{-6} to $12.5 \times 10^{-6} K^{-1}$, compatible to chromia which has the TEC of about $9.6 \times 10^{-6} K^{-1}$ at 25–900 °C [10] and Fe–20Cr ferritic stainless steel which has the TEC of about $12.5 \times 10^{-6} K^{-1}$ at 800 °C [105]. The exception is $ZnFe_2O_4$ which its TEC is relatively lower i.e. $7 \times 10^{-6} K^{-1}$. However, it is noticed that some other spinels i.e. $Cu_{1.3}Mn_{1.7}O_4$, $MnCo_2O_4$ and $CuCo_2O_4$ also have the TECs of 12.2×10^{-6} , 9.7×10^{-6} , $11.2 \times 10^{-6} K^{-1}$, respectively, close to those of chromia and Fe–20Cr ferritic stainless steel.

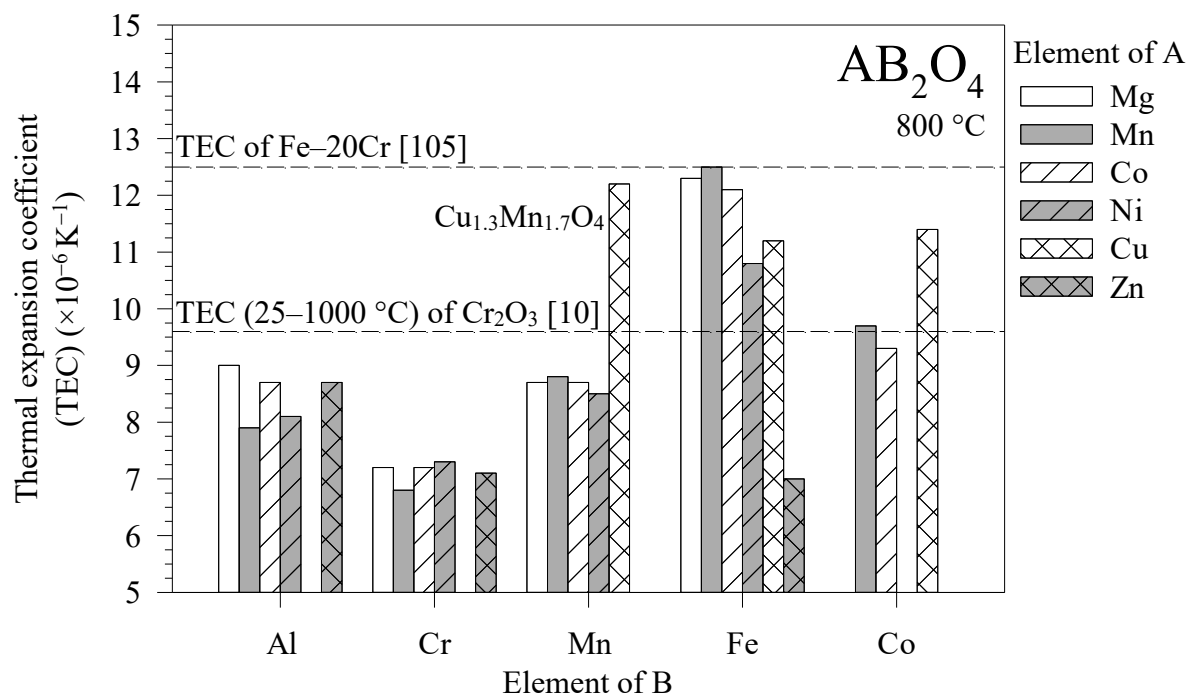


Fig. 6.5. Thermal expansion coefficients of different AB_2O_4 spinels at 800 °C [10, 103–105].

Figs. 6.6 (a) and (b) present electrical conductivities of the spinels. All spinels in the figures have a formula of AB_2O_4 and their conductivities were measured at 800 °C. The exception is Cu–Mn spinel which has a formula of $Cu_{1.3}Mn_{1.7}O_4$ and its conductivity was measured at 750 °C. It can be seen that the electrical conductivities of spinels in Fig. 6.6(a) are less than 1.5 S cm^{-1} . In Fig. 6.6(b), it is seen that $Cu_{1.3}Mn_{1.7}O_4$ exhibits the highest value of the electrical conductivity of about 225 S cm^{-1} even though the test temperature was lower than those of the other spinels. At 800 °C, $MnCo_2O_4$ and $CuCo_2O_4$ exhibit the relatively high values of the electrical conductivities of about 60 S cm^{-1} and 27.5 S cm^{-1} respectively. As mentioned in the former paragraph, these three spinels also have the TECs close to those of the chromia and Fe–20Cr ferritic stainless steel. $Cu_{1.3}Mn_{1.7}O_4$, $MnCo_2O_4$ and $CuCo_2O_4$ are then promising to be used as coating material for the present application.

As for the examples of the spinel coatings, Yang coated $Mn_{1.5}Co_{1.5}O_4$ on Crofer 22 APU [97, 99, 106]. After the exposure at 800 °C in air, ASR of the uncoated material was $40 \text{ m}\Omega \text{ cm}^2$ after 400 h [97, 106], similar to the results shown in Fig. 6.3. The coating could reduce the ASR to $10 \text{ m}\Omega \text{ cm}^2$ even after the exposure for 1000 h [97, 106]. After the longer exposure for 6 months under thermal cycling, the coating was found to be well adhered to the substrate and the sharp, thin profile of chromium across the interface between the subscale and spinel coating was observed [99, 106].

However, in some cases the spinel coating could also increase the chromium species volatilisation rate, such as the case of Cr–Mn spinel coating on AISI 441 conducted by Wongromrat et al. [5]. The discussion was made that the formation of chromium volatile species according to Reaction 6.9 might be from the non-elementary steps as shown in Reactions 6.14–6.16. In this mechanism, oxygen gas in the atmosphere may adsorb on the solid surface according to Reaction 6.14 or directly react with chromia to form CrO_2^{2+} according to Reaction 6.16. The adsorbed oxygen gas is reduced giving hydroxide ion according to Reaction 6.15. It was reported that the Mn–Co spinel is one of the good electrocatalysts for oxygen reduction found in the alkaline battery [5, 107, 108]. It is then possible that Reaction 6.15 is enhanced. If Reaction 6.15 is a rate determining step for the overall chromium species volatilisation, the increased rate of Reaction 6.15 then increases the overall rate of the chromium species volatilisation.

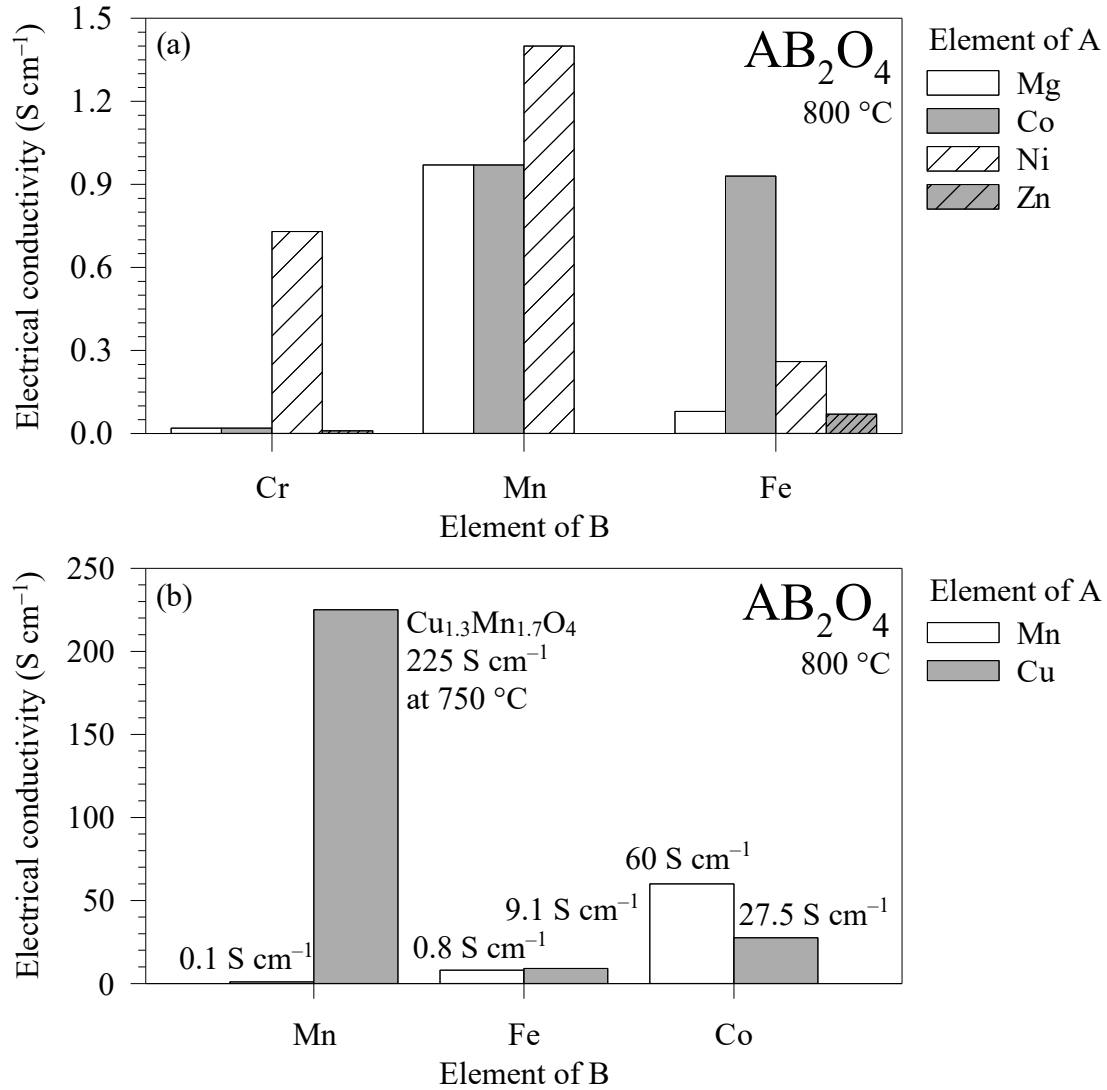


Fig. 6.6. Electrical conductivities of different AB_2O_4 spinels at 800 °C [103, 104].



Recently, new strategies have been proposed in order to increase the oxidation resistance as well as the electrical conductivity. This new evolution in coating approach consists in associating several types of coatings in order to obtain positive properties from each of them. As an example, Balland et al. [109] pre-covered a Crofer steel by La_2O_3 , performed an annealing treatment in order to form $LaCrO_3$ perovskite coating prior to deposit metallic (Co,Mn) films. During aging of the coated samples, the metallic (Co,Mn) film transformed into $(Co,Mn)_3O_4$ which guaranteed good electrical conductivity. These duplex coatings inhibited both chromia sublayer formation (compared to the single $(Co,Mn)_3O_4$ layer) and the formation of iron oxide in dual atmosphere exposures (compared to the single La_2O_3).

6.8 Conclusions and Perspectives

The SOFC working temperature has been aimed at reducing to 800 °C or lower. Thus the application of stainless steel as an interconnect becomes possible. A ferritic stainless steel is selected for this application because of the compatibility of its thermal expansion coefficient (TEC) with a single cell. Chromia-forming stainless steel is further selected instead of the alumina-forming one to avoid the formation of insulating alumina during oxidation. The required properties of ferritic stainless steel for this application are not only the TEC compatibility and high electrical conductivity of the oxide formed at high temperatures, but also its low oxidation rate, low chromium species volatilisation and good scale adhesion in the SOFC environment.

The steel grades for this application start from stainless steel with chromium of about 16 wt.% (AISI 430) and up to the grades with higher chromium content of about 18 wt.% (e.g. AISI 441) and 22 wt.% (e.g. Crofer 22 APU and ZMG 232). Stabilisers and reactive elements can be added to the steel such as titanium and niobium in AISI 441, titanium and lanthanum in Crofer 22 APU, or zirconium and lanthanum in ZMG 232. Coating is recommended to be applied on steel surface in order to reduce the oxidation rate, avoid chromium species volatilisation and increase electrical conductivity of the steel. The promising coating materials are such as spinels e.g. Mn–Co, Cu–Mn or Cu–Co spinels, as well as perovskites.

The tendency of SOFC development is to operate it at lower temperatures e.g. towards 600 °C. The possibility to use the fossil fuel in SOFCs requires the basic understanding in reactivity of interconnect materials in such environments, followed by the development of protective coatings.

References

- [1] P. Kofstad, R. Bredesen, High temperature corrosion in SOFC environments, *Solid State Ionics* 52 (1992) 69–75.
- [2] K. Kendall, Chapter 1 Introduction to SOFCs, in: K. Kendall, M. Kendall (Eds.), *High-Temperature Solid Oxide Fuel Cells for the 21st Century: Fundamental, Design and Applications*, second ed., Academic Press, UK, 2016, pp. 1–24.
- [3] S.C. Singhal, Solid oxide fuel cells for stationary, mobile, and military applications, *Solid State Ionics* 152–153 (2002) 405–410.
- [4] L. Antoni, Materials for solid oxide fuel cells: the challenge of their stability, *Mater. Sci. Forum* 461–464 (2004), 1073–1090.
- [5] W. Wongpromrat, H. Thaikhan, W. Chandra-ambhorn, S. Chandra-ambhorn, Chromium vaporisation from AISI 441 stainless steel oxidised in humidified oxygen, *Oxid. Met.* 79 (2013) 529–540.
- [6] W. Wongpromrat, G. Berthomé, V. Parry, S. Chandra-ambhorn, W. Chandra-ambhorn, C. Pascal, A. Galerie, Y. Wouters, Reduction of chromium volatilisation from stainless steel interconnector of solid oxide electrochemical devices by controlled peroxidation, *Corros. Sci.* 106 (2016) 172–178.
- [7] I. Barin, *Thermochemical Data of Pure Substances*, VCH, Germany, 1989.
- [8] J. Kupecki, K. Motylinski, J. Milewski, Dynamic analysis of direct internal reforming in a SOFC stack with electrolyte-supported cells using a quasi-1D model, *Appl. Energy* 227 (2018) 198–205.
- [9] W.Z. Zhu, S.C. Deevi, Opportunity of metallic interconnects for solid oxide fuel cells: a status on contact resistance, *Mater. Res. Bull.* 38 (2003), 957–972.
- [10] W.Z. Zhu, S.C. Deevi, Development of interconnect materials for solid oxide fuel cells, *Mater. Sci. Eng., A* 348 (2003), 227–243.
- [11] V. Shemet, J. Piron-Abellan, W. J. Quadackers, L. Singheiser, Metallic materials in solid oxide fuel cells, in: N. Sammes, A. Smirnova, O. Vasylyev (Eds.), *Fuel Cell Technologies: State and Perspectives*, Springer, The Netherlands, 2005, pp. 97–106.

-
- [12] Z. Yang, Recent advances in metallic interconnects for solid oxide fuel cells, *Int. Mater. Rev.* 53 (2008) 39–54.
- [13] J.W. Fergus, Lanthanum chromite-based materials for solid oxide fuel cell interconnects, *Solid State Ionics* 171 (2004) 1–15.
- [14] S.P.S. Badwal, Stability of solid oxide fuel cell components, *Solid State Ionics* 143 (2001), 39–46.
- [15] K. Hilpert, R.W. Steinbrech, F. Boroomand, E. Wessel, F. Meschke, A. Zuev, O. Teller, H. Nickel, L. Singheiser, Defect formation and mechanical stability of perovskites based on LaCrO_3 for solid oxide fuel cells (SOFC), *J. Eur. Ceram. Soc.* 23 (2003) 3009–3020.
- [16] S. de Souza, S.J. Visco, L.C. De Jonghe, Thin-film solid oxide fuel cell with high performance at low-temperature, *Solid State Ionics* 98 (1997) 57–61.
- [17] F. Mauvy, J.-M. Bassat, E. Boehm, J.-P. Manaud, P. Dordor, J.-C. Grenier, Oxygen electrode reaction on $\text{Nd}_2\text{NiO}_{4+\delta}$ cathode materials: impedance spectroscopy study, *Solid State Ionics* 158 (2003) 17–28.
- [18] J.W. Fergus, Metallic interconnects for solid oxide fuel cells, *Mater. Sci. Eng. A* 397 (2005) 271–283.
- [19] Z. Yang, K.S. Weil, D.M. Paxton J.W. Stevenson, Selection and evaluation of heat-resistant alloys for SOFC interconnect applications, *J. Electrochem. Soc.* 150 (2003) A1188–A1201.
- [20] M. Bianco, M. Linder, Y. Larring, F. Greco, J. Van herle, Chapter 7 Lifetime issues for solid oxide fuel cell interconnects, in: N.P. Brandon, E. Ruiz-Trejo, P. Boldrin (Eds.), *Solid Oxide Fuel Cell Lifetime and Reliability: Critical Challenges in Fuel Cells*, Academic Press, UK, 2017, pp. 121–144.
- [21] W.J. Quadackers, J. Piron-Abellan, V. Shemet, L. Singheiser, Metallic interconnectors for solid oxide fuel cells – a review, *Mater. High Temp.* 20 (2003) 115–127.
- [22] W.J. Quadackers, H. Greiner, W. Köck, Metals and alloys for high temperature SOFC application, in: U. Bossel (Ed.), *Proceedings of the First European Solid Oxide Fuel Cell Forum Vol. 1*, European Fuel Cell Forum, Switzerland, 1994, pp. 525–544.
- [23] C. Hatchwell, N.M. Sammes, I.W.M. Brown, K. Kendall, Current collectors for a novel tubular design of solid oxide fuel cell, *J. Power Sources* 77 (1999) 64–68.
- [24] H.P. Buchkremer, U. Diekmann, L.G.J. de Haart, H. Kabs, D. Stöver, I.C. Vinke, Advances in manufacturing and operation of anode supported SOFC cells and stacks, in: P. Stevens (Ed.), *Proceedings of the Third European Solid Oxide Fuel Cell Forum*, European Fuel Cell Forum, France, 1998, pp. 143–149.
- [25] J.P. Abellán, V. Shemet, F. Tietz, L. Singheiser, W.J. Quadackers, A. Gil, Ferritic steel interconnect for reduced temperature SOFC, in: H. Yokokawa, S.C. Singhal (Eds.), *Proceedings of The Electrochemical Society PV 2001-16 (SOFC–VII)*, The Electrochemical Society, USA, 2001, pp. 811–819.
- [26] K. Hilpert, D. Das, M. Miller, D.H. Peck, R. Weiß, Chromium vapor species over solid oxide fuel cell interconnect materials and their potential for degradation processes, *J. Electrochem. Soc.* 143 (1996) 3642–3647.
- [27] H. Yokokawa, T. Horita, N. Sakai, K. Yamaji, M.E. Brito, X.-P. Xiong, H. Kishimoto, Thermodynamic considerations on Cr poisoning in SOFC cathodes, *Solid State Ionics* 177 (2006) 3193–3198.

- [28] R.E. Lobnig, H.P. Schmidt, K. Hennesen, H.J. Grabke, Diffusion of cations in chromia layers grown on iron-base alloys, *Oxid. Met.* 37 (1992) 81–93.
- [29] W. Qu, J. Li, D.G. Ivey, Sol–gel coatings to reduce oxide growth in interconnects used for solid oxide fuel cells, *J. Power Sources* 138 (2004) 162–173.
- [30] E. Konysheva, U. Seeling, A. Besmehn, L. Singheiser, K. Hilpert, Chromium vaporization of the ferritic steel Crofer22APU and ODS Cr5Fe1Y₂O₃ alloy, *J. Mater. Sci.* 42 (2007) 5778–5784.
- [31] G.R. Holcomb, D.E. Alman, The effect of manganese additions on the reactive evaporation of chromium in Ni–Cr alloys, *Scr. Mater.* 54 (2006) 1821–1825.
- [32] D.L. Douglass, J.S. Armijo, The influence of manganese and silicon on the oxidation behavior of Co–20Cr, *Oxid. Met.* 3 (1971) 185–202.
- [33] L. Mikkelsen, S. Linderöth, J.B. Bilde-Sørensen, The effect of silicon addition on the high temperature oxidation of a Fe–Cr alloy, *Mater. Sci. Forum* 461–464 (2004) 117–122.
- [34] P.D. Jablonski, D.E. Alman, Oxidation resistance of novel ferritic stainless steels alloyed with titanium for SOFC interconnect applications, *J. Power Sources* 180 (2008) 433–439.
- [35] T. Horita, H. Kishimoto, K. Yamaji, Y. Xiong, N. Sakai, M.E. Brito, H. Yokokawa, Evaluation of laves-phase forming Fe–Cr alloy for SOFC interconnects in reducing atmosphere, *J. Power Sources* 176 (2008) 54–61.
- [36] S. Chandra-ambhorn, Y. Wouters, L. Antoni, F. Toscan, A. Galerie, Adhesion of oxide scales grown on ferritic stainless steels in solid oxide fuel cells temperature and atmosphere conditions, *J. Power Sources* 171 (2007) 688–695.
- [37] L. Niewolak, F. Tietz, W.J. Quadackers, Chapter 7 Interconnect, in: K. Kendall, M. Kendall (Eds.), *High-Temperature Solid Oxide Fuel Cells for the 21st Century: Fundamental, Design and Applications*, second ed., Academic Press, UK, 2016, pp. 195–254.
- [38] T. Uehara, N. Yasuda, T. Ohno, A. Toji, Improvement of oxidation resistance of Fe–Cr ferritic alloy sheets for SOFC interconnects, *Electrochem.* 77 (2009) 131–133.
- [39] K. Yamamura, T. Uehara, Long term oxidation resistance of Fe–Cr ferritic steel ZMG232G10 for SOFC interconnects, in: I. Saeki (Ed.), *Proceedings of the International Symposium on High-Temperature Oxidation and Corrosion 2018 (ISHOC 2018)*, Japan, 2018, pp. 246–249.
- [40] A. Galerie, High temperature corrosion of chromia-forming iron, nickel and cobalt-base alloys, in: R.A. Cottis, M.J. Graham, R. Lindsay, S.B. Lyon, J.A. Richardson, J.D. Scantlebury, F.H. Stott (Eds.), *Shreir's Corrosion*, forth ed., Elsevier, The Netherlands, 2010, pp. 583–605.
- [41] S.S.M. Tavares, J.A. de Souza, L.F.G. Herculano, H.F.G. de Abreu, C.M. de Souza Jr., Microstructural, magnetic and mechanical property changes in an AISI 444 stainless steel aged in the 560 °C to 800 °C range, *Mater. Charact.* 59 (2008) 112–116.
- [42] T. Juuti, L. Rovatti, A. Mäkelä, L.P. Kajalainen, D. Porter, Influence of long heat treatments on the laves phase nucleation in a type 444 ferritic stainless steel, *J. Alloys. Compd.* 616 (2014) 250–256.
- [43] V. Villaret, F. Deschaux-Beaume, C. Bordreuil, S. Rouquette, C. Chovet, Influence of filler wire composition on weld microstructures of a 444 ferritic stainless steel grade, *J. Mater. Proc. Technol.* 213 (2013) 1538–1547.
- [44] A. Miyasaka, J. Hirasawa, O. Furukimi, Development of high heat-resistant ferritic stainless steel with high formability, “RMH-1,” for automotive exhaust manifolds by optimizing Mo composition design, *Kawasaki Steel Technical Report* 48 (2003) 28–32.

-
- [45] J.H. Potgieter, M. Sephton, Z.W. Nkosi, Corrosion of hot and automotive exhaust components, *Anti-Corros. Methods Mater.* 54 (2007) 180–187.
- [46] L. Singheiser, P. Huczowski, T. Markus, W.J. Quaddakers, High temperature issues for metallic materials in solid oxide fuel cells, in: R.A. Cottis, M.J. Graham, R. Lindsay, S.B. Lyon, J.A. Richardson, J.D. Scantlebury, F.H. Stott (Eds.), *Shreir's Corrosion*, forth ed., Elsevier, The Netherlands, 2010, pp. 482–517.
- [47] S. Chevalier, G. Bonnet, G. Borchardt, J.C. Colson, J.P. Larpin, Mechanisms involved by reactive elements upon high temperature chromia scale growth, *Mater. Sci. Forum* 369–372 (2001) 327–336.
- [48] P.Y. Hou, J. Stringer, The effect of reactive element additions on the selective oxidation, growth and adhesion of chromia scales, *Mater. Sci. Eng. A* 202 (1995) 1–10.
- [49] M. Park, J.-S. Shin, S. Lee, H.-J. Kim, H. An, H.-I. Ji, H. Kim, J.-W. Son, J.-H. Lee, B.-K. Kim, H.-W. Lee, K.J. Yoon, Thermal degradation mechanism of ferritic alloy (Crofer 22 APU), *Corros. Sci.* 134 (2018) 17–22.
- [50] G. Cabouro, G. Caboche, S. Chevalier, P. Piccardo, Opportunity of metallic interconnects for ITSOFC: reactivity and electrical property, *J. Power Sources* 156 (2006) 39–44.
- [51] S. Fontana, S. Chevalier, G. Caboche, Metallic interconnects for solid oxide fuel cell: performance of reactive element oxide coating during 10, 20 and 30 months exposure, *Oxid. Met.* 78 (2012) 307–328.
- [52] K. Przybylski, A.J. Garratt-Reed, G.J. Yurek, Grain boundary segregation of yttrium in chromia scales, *J. Electrochem. Soc.* 135 (1988) 509–517.
- [53] S. Fontana, S. Chevalier, G. Caboche, Metallic interconnects for solid oxide fuel cell: effect of water vapour on oxidation resistance of differently coated alloys, *J. Power Sources* 193 (2009) 136–145.
- [54] S.R.J. Saunders, M. Monteiro, F. Rizzo, The oxidation behaviour of metals and alloys at high temperatures in atmospheres containing water vapour: a review, *Prog. Mater. Sci.* 53 (2008) 775–837.
- [55] T. Brylewski, M. Nanko, T. Maruyama, K. Przybylski, Application of Fe–16Cr ferritic alloy to interconnector for a solid oxide fuel cell, *Solid State Ionics* 143 (2001) 131–150.
- [56] W.J. Quadackers, T. Malkow, J. Pirón-Abellán, U. Flesch, V. Shemet, Suitability of ferritic steels for application as construction material for SOFC interconnects, in: A.J. McEvoy (Ed.), *Proceedings of the Fourth Solid Oxide Fuel Cell Forum Vol. 2*, European Fuel Cell Forum, Switzerland, 2000, pp. 827–836.
- [57] D.M. England, A.V. Virkar, Oxidation kinetics of some nickel-based superalloy foils in humidified hydrogen and electronic resistance of the oxide scale formed: part II, *J. Electrochem. Soc.* 148 (2001) A330–A338.
- [58] Y. Liu, Performance evaluation of several commercial alloys in a reducing environment, *J. Power Sources* 179 (2008) 286–291.
- [59] S. Guillou, C. Desgranges, S. Chevalier, Study of conductivity of K41X chromia forming alloy in high temperature electrolysis environment, *Oxid. Met.* 79 (2013), 507–516.
- [60] Y. Larring, R. Haugsrud, T. Norby, HT corrosion of a Cr-5 wt % Fe-1 wt % Y_2O_3 alloy and conductivity of the oxide scale: effects of water vapour, *J. Electrochem. Soc.* 150 (2003) B374–B379.
- [61] M. Hänsel, W.J. Quadackers, D.J. Young, Role of water vapor in chromia-scale growth at low oxygen partial pressure, *Oxid. Met.* 59 (2003) 285–301.

- [62] S. Rasi, V. Veijanen, J. Rintala, Trace compounds of biogas from different biogas production plants, *Energy* 32 (2007) 1375–1380.
- [63] P. Promdirek, G. Lothongkum, S. Chandra-ambhorn, Y. Wouters, A. Galerie, Behaviour of ferritic stainless steels subjected to dry biogas atmospheres at high temperatures, *Mater. Corros.* 62 (2011) 616–622.
- [64] P. Promdirek, G. Lothongkum, S. Chandra-ambhorn, Y. Wouters, A. Galerie, Oxidation kinetics of AISI 441 ferritic stainless steel at high temperatures in CO₂ atmosphere, *Oxid. Met.* 81 (2014) 315–329.
- [65] Z. Yang, M.S. Walker, P. Singh, J.W. Stevenson, Anomalous corrosion behavior of stainless steels under SOFC interconnect exposure conditions, *Electrochem. Solid-State Lett.* 6 (2003) B35–B37.
- [66] Z. Yang, M.S. Walker, P. Singh, J.W. Stevenson, T. Norby, Oxidation behavior of ferritic stainless steels under SOFC interconnect exposure conditions, *J. Electrochem. Soc.* 151 (2004) B669–B678.
- [67] G.R. Holcomb, M. Ziomek-Moroz, S.D. Cramer, B.S. Covino Jr., S.J. Bullard, Dual-environment effects on the oxidation of metallic interconnects, *J. Mater. Eng. Perform.* 15 (2006) 404–409.
- [68] T. Horita, H. Kishimoto, K. Yamaji, N. Sakai, Y. Xiong, M.E. Brito, H. Yokokawa, Anomalous oxidation of ferritic interconnects in solid oxide fuel cells, *Int. J. Hydrogen Energy* 33 (2008) 3962–3969.
- [69] Y.-S. Chou, J.W. Stevenson, G.-G. Xia, Z.-G. Yang, Electrical stability of a novel sealing glass with (Mn,Co)-spinel coated Crofer22APU in a simulated SOFC dual environment, *J. Power Sources* 195 (2010) 5666–5673.
- [70] R. Amendola, P. Gannon, B. Ellingwood, K. Hoyt, P. Piccardo, P. Genocchio, Oxidation behavior of coated and preoxidized ferritic steel in single and dual atmospheres at 800 °C, *Surf. Coat. Technol.* 206 (2012) 2173–2180.
- [71] P. Gannon, R. Amendola, High-temperature, dual-atmosphere corrosion of solid-oxide fuel cell interconnects, *JOM* 64 (2012) 1470–1476.
- [72] A.W.B. Skilbred, R. Haugsrud, The effect of dual atmosphere conditions on the corrosion of Sandvik Sanergy HT, *Int. J. Hydrogen Energy* 37 (2012) 8095–8101.
- [73] K. Kawamura, T. Nitobe, H. Kurokawa, M. Ueda, T. Maruyama, Effect of electric current on growth of oxide scale on Fe–25Cr alloy for SOFC interconnect at 1073 K, *J. Electrochem. Soc.* 159 (2012) B259–B264.
- [74] Y. Zhao, J.W. Fergus, Oxidation of alloys 430 and 441 in SOFC dual atmospheres: effects of flow rate and humidity, *J. Electrochem. Soc.* 159 (2012) C109–C113.
- [75] M.G.C. Cox, B. Mcenaney, V.D. Scott, A chemical diffusion model for partitioning of transition elements in oxide scales on alloys, *Phil. Mag.* 26 (1972) 839–851.
- [76] H. Kurokawa, Y. Oyama, K. Kawamura, T. Maruyama, Hydrogen permeation in Fe–16Cr alloy in the atmosphere simulating SOFC at 1073 K, in: E. Opila, P. Hou, T. Maruyama, B. Pieraggi, D. Shifler, E. Wuchina (Eds.), *High Temperature Corrosion and Materials Chemistry IV*, The Electrochemical Society, USA, 2003, pp. 170–177.
- [77] M.R. Ardigo, I. Popa, L. Combemale, S. Chevalier, F. Herbst, P. Girardon, Dual atmosphere study of the K41X stainless steel for interconnect application in high temperature water vapour electrolysis, *Int. J. Hydrogen Energy* 40 (2015) 5305–5312.

- [78] E.J. Opila, D.L. Myers, N.S. Jacobson, I.M.B. Nielsen, D.F. Johnson, J.K. Olminky, M.D. Allendorf, Theoretical and experimental investigation of the thermochemistry of $\text{CrO}_2(\text{OH})_{2(g)}$, *J. Phys. Chem. A* 111 (2007) 1971–1980.
- [79] N.H. Menzler, P. Batfalsky, S.M. Groß, V. Shemet, F. Tietz, Post-test characterization of an SOFC short stack after 17,000 hours of steady operation, *ECS Trans.* 35 (2011) 195–206.
- [80] H. Falk-Windisch, J.E. Svensson, J. Froitzheim, The effect of temperature on chromium vaporization and oxide scale growth on interconnect steels for solid oxide fuel cells, *J. Power Sources* 287 (2015) 25–35.
- [81] N. Mahato, A. Banerjee, A. Gupta, S. Omar, K. Balani, Progress in material selection for solid oxide fuel cell technology: a review, *Prog. Mater. Sci.* 72 (2015) 141–337.
- [82] Z. Yang, M. Guo, N. Wang, C. Ma, J. Wang, M. Han, A short review of cathode poisoning and corrosion in solid oxide fuel cell, *Int. J. Hydrogen Energy*. 42 (2017) 24948–24959.
- [83] I.-H. Jung, Critical evaluation and thermodynamic modeling of the Mn–Cr–O system for the oxidation of SOFC interconnect, *Solid State Ionics* 177 (2006) 765–777.
- [84] M. Stanislawski, E. Wessel, K. Hilpert, T. Markus, L. Singheiser, Chromium vaporization from high-temperature alloys: I. chromia-forming steels and the influence of outer oxide layers, *J. Electrochem. Soc.* 154 (2007) A295–A306.
- [85] R. Suchitanand, M. Sattari, J.-E. Svensson, J. Froitzheim, Evaluation of the oxidation and Cr evaporation properties of selected FeCr alloys used as SOFC interconnects, *Int. J. Hydrogen Energy*. 38 (2013) 15328–15334.
- [86] S. Chandra-ambhorn, Reactivity and surface modification of stainless steels used as electric interconnectors in high temperature solid oxide fuel cells, PhD Thesis, INP Grenoble, France, 2006.
- [87] K. Huang, P.Y. Hou, J.B. Goodenough, Characterization of iron-based alloy interconnects for reduced temperature solid oxide fuel cells, *Solid State Ionics* 129 (2000) 237–250.
- [88] P. Piccardo, P. Gannon, S. Chevalier, M. Viviani, A. Barbucci, G. Coboche, R. Amendola, S. Fontana, ASR evaluation of different kinds of coatings on a ferritic stainless steel as SOFC interconnects, *Surf. Coat. Technol.* 202 (2007) 1221–1225.
- [89] H. Ebrahimifar, M. Zandrahimi, Oxidation and electrical behavior of AISI 430 coated with cobalt spinels for SOFC interconnect applications, *Surf. Coat. Technol.* 206 (2011) 75–81.
- [90] N. Shaigan, D.G. Ivey, W. Chen, Co/LaCrO₃ composite coatings for AISI 430 stainless steel solid oxide fuel cell interconnects, *J. Power Sources* 185 (2008) 331–337.
- [91] W.J. Quaddakers, J. Pirón-Abellán, V. Shemet, Metallic materials in solid oxide fuel cells, *Mater. Res.* 7 (2004) 203–208.
- [92] J.G. Grolig, J. Froitzheim, J.-E. Svensson, Coated stainless steel 441 as interconnect material for solid oxide fuel cells: evolution of electrical properties, *J. Power Sources* 284 (2015) 321–327.
- [93] S.N. Hosseini, F. Karimzadeh, M.H. Enayati, N.M. Sammes, Oxidation and electrical behavior of CuFe_2O_4 spinel coated Crofer 22 APU stainless steel for SOFC interconnect application, *Solid State Ionics* 289 (2016) 95–105.
- [94] H. Ebrahimifar, M. Zandrahimi, Oxidation and electrical behavior of Mn-Co-coated Crofer 22 APU steel produced by a pack cementation method for SOFC interconnect applications, *Oxid. Met.* 84 (2015) 129–149.

- [95] A. Galerie, M.R. Ardigo, P. Berthod, W. Chandra-ambhorn, S. Chevalier, P.Y. Hou, F. Rouillard, Chapter 1 Influence of water vapor on high-temperature oxidation of chromia-forming materials, in: S. Chevalier, J. Favergeon (Eds.), French Activity on High Temperature Corrosion in Water Vapor, Trans Tech Publications, Switzerland, 2014, pp. 1–25.
- [96] J.C.W. Mah, A. Muchtar, M.R. Somalu, M.J. Ghazali, Metallic interconnects for solid oxide fuel cell: a review on protective coating and deposition techniques, *Int. J. Hydrogen Energy* 42 (2017) 9219–9229.
- [97] J. Wu, X. Liu, Recent Development of SOFC Metallic Interconnect, *J. Mater. Sci. Technol.* 26 (2010) 293–305.
- [98] J.-L. Choi, B.-K. Park, S.-B. Lee, R.-H. Song, J.-W. Lee, Efficient and robust ceramic interconnects based on a mixed-cation perovskite for solid oxide fuel cells, *Ceram. Int.* 45 (2019) 4902–4908.
- [99] N. Shaigan, W. Qu, D.G. Ivey, W. Chen, A review of recent progress in coatings, surface modifications and alloy developments for solid oxide fuel cell ferritic stainless steel interconnects, *J. Power Sources* 195 (2010) 1529–1542.
- [100] S. Fontana, S. Chevalier, G. Caboche, Metallic interconnects for solid oxide fuel cell: performance of reactive element oxide coating during long time exposure, *Mater. Corros.* 62 (2011) 650–658.
- [101] S. Chevalier, G. Bonnet, K. Przybylski, J.C. Colson, J.P. Larpin, Segregation of neodymium in chromia grain-boundaries during high-temperature oxidation of neodymium oxide-coated chromia-forming alloys, *Oxid. Met.* 54 (2000) 527–547.
- [102] S. Chevalier, *Traitements de surface et nouveaux matériaux: Quelles solutions pour lutter contre la dégradation des matériaux à haute température ?*, Les Editions Universitaires de Dijon, France, 2007.
- [103] A. Petric, H. Ling, Electrical conductivity and thermal expansion of spinels at elevated temperatures, *J. Am. Ceram. Soc.* 90 (2007) 1515–1520.
- [104] P. Paknahad, M. Askari, M. Ghorbanzadeh, Application of sol–gel technique to synthesis of copper–cobalt spinel on the ferritic stainless steel used for solid oxide fuel cell interconnects, *J. Power Sources* 266 (2014) 79–87.
- [105] S. Linderoth, P.H. Larsen, Investigations of Fe–Cr ferritic steels as SOFC interconnect material, *MRS Proc.* 575 (1999) 325–330.
- [106] Z. Yang, G. Xia, S.P. Simmer, J. Stevenson, Thermal growth and performance of manganese cobaltite spinel protection layers on ferritic stainless steel SOFC interconnects, *J. Electrochem. Soc.* 152 (2005) A1896–A1901.
- [107] A. Restovic, E. Ríos, S. Barbato, J. Ortiz, J.L. Gautier, Oxygen reduction in alkaline medium at thin $\text{Mn}_x\text{Co}_{3-x}\text{O}_4$ ($0 \leq x \leq 1$) spinel films prepared by spray pyrolysis. Effect of oxide cation composition on the reaction kinetics, *J. Electroanal. Chem.* 522 (2002) 141–151.
- [108] E. Ríos, H. Reyes, J. Ortiz, J.L. Gautier, Double channel electrode flow cell application to the study of HO_2^- production on $\text{Mn}_x\text{Co}_{3-x}\text{O}_4$ ($0 \leq x \leq 1$) spinel films, *Electrochim. Acta* 50 (2005) 2705–2711.
- [109] A. Balland, P. Gannon, M. Deibert, S. Chevalier, G. Caboche, S. Fontana, Investigation of La_2O_3 and/or $(\text{Co},\text{Mn})_3\text{O}_4$ deposits on Crofer22APU for the SOFC interconnect application, *Surf. Coat. Technol.* 203 (2009) 3291–3296.